ECS Transactions, 85 (5) 43-64 (2018)
10.1149/08505.0043ecst ©The Electrochemical Society

Estimation of Transport and Kinetic Parameters of Vanadium Redox Batteries Using Static Cells

Seong Beom Lee[a], Harry D. Pratt III[b], Travis M. Anderson[b], Kishalay Mitra[c], Babu R. Chalamala[b], and Venkat R. Subramanian[a, d]

[a] Department of Chemical Engineering, University of Washington, Seattle, WA 98195, USA
[b] Sandia National Laboratories, Albuquerque, NM 87185, USA
[c] Department of Chemical Engineering, Indian Institute of Technology Hyderabad, Kandi, Sangareddy, Telangana 502285, INDIA
[d] Pacific Northwest National Laboratory, Richland, WA 99354, USA

Mathematical models of Redox Flow Batteries (RFBs) can be used to analyze cell performance, optimize battery operation, and control the energy storage system efficiently. Among many other models, physics-based electrochemical models are capable of predicting internal states of the battery, such as temperature, state-of-charge, and state-of-health. In the models, estimating parameters is an important step that can study, analyze, and validate the models using experimental data. A common practice is to determine these parameters either through conducting experiments or based on the information available in the literature. However, it is not easy to investigate all proper parameters for the models through this way, and there are occasions when important information, such as diffusion coefficients and rate constants of ions, has not been studied. Also, the parameters needed for modeling charge-discharge are not always available. In this paper, an efficient way to estimate parameters of physics-based redox battery models will be proposed. This paper also demonstrates that the proposed approach can study and analyze aspects of capacity loss/fade, kinetics, and transport phenomena of the RFB system.

Introduction

Redox Flow Batteries (RFBs) are promising energy storage systems for grid/microgrid applications (1). There has been significant technological progress in the recent past towards meeting the growing need for large-scale energy storage systems for RFBs (2). Among different types of RFBs, Vanadium Redox Flow Batteries (VRFBs) have gained more attention, and as a result of this, several physics-based electrochemical models for these systems describing the physics of the battery operations have been developed (3-12).

Physics-based electrochemical models can be classified by dimensions, from zero- to two-dimensional models as shown in Table I. Models in each category have their own advantages and can be used depending on users' purposes. For example, zero-dimensional models have been developed to be easy to implement, enabling to quickly understand, predict, and control the battery system (9, 13). Multi-dimensional models have been implemented with the more detailed physics of the system (3). As described in Table I, the current trend is to include more ions and detailed physical phenomena, such as transport of ions and side reactions of the system (8, 12), and therefore models with further complexities have been built. Most

models are still based on isothermal effects and dilute solution theories. For zero-dimensional models, a model was developed for static cell systems, including diffusion of vanadium ions through the membrane (11), and this was the first attempt of the zero-dimensional models to simulate ions crossover through the membrane (11). The model was further developed to models that include all ions and transports of the system (3, 13). For one-dimensional models, one-dimensional membrane models based on dilute and concentrated solution theories have been developed assuming bulk electrolytes at positive and negative (14, 15). For two-dimensional case, flow cell models have been developed to include diffusion, migration, and convection of all ions and detailed physics of the system (3).

An efficient way of combining physics-based electrochemical models and parameters estimation techniques can facilitate the research on energy storage technologies which are indispensable for the success of intermittent sources of energy. For instance, the current practice in the grid/microgrid control systems is to utilize empirical battery models regardless of the types of the batteries (16). More extended battery life and reduction in the size of RFBs, which are two of the most critical factors in battery control system, can be achieved better if these empirical battery models are replaced with physics-based electrochemical models. The physics-based models have the power of predicting the battery performance and internal states accurately. With such detailed models, an efficient equation-based PV-Battery microgrid framework was recently developed that can implement any kind of physics-based electrochemical battery models (17). Once the specific battery models are incorporated into the efficient equation-based microgrid framework, an important task is to estimate the parameters used in the model. The values of these parameters need updating at certain regular intervals to reflect the change in battery behavior over the cycles of charging/discharging. This enables the models to have accurate predictions for several states of battery parameters, leading to a better prediction of battery usability and life. The proper estimation of parameters with physics-based battery models can maximize battery life and usability. It also helps analyze and study the kinetics of ions, transport phenomena, and capacity fade/loss of the cell system. However, several attempts to estimate the states and parameters of VRFB system have been made using empirical/equivalent circuit-based models, which do not include physics of the battery in details.(18-20) Also, other research works collect most of the parameters from the experimental literature and estimate one or two remaining parameters in mathematical models (3, 9). However, many of these experiments require either physical destruction of the battery or tedious as well as sophisticated experimental setup (21-23). For example, dialysis cell, pumps, and measuring cylinder are utilized to investigate diffusion coefficients of ions through a membrane in an RFB experimental setup (24). Also, a design of a sophisticated experiment, including a linear sweep voltammetry and electrochemical impedance spectroscopy, was used to investigate reaction rate information for the kinetic parameters at electrodes (25, 26).

In this paper, we show that the proposed estimation approach can help study and analyze important aspects of redox batteries, such as capacity fade/loss, kinetics, and transport of ions, including physics-based battery models for a laboratory-scale static cell system. The laboratory-scale static cell system, consisting of a transparent H-cell, a membrane, electrolytes, and electrodes, has been used to study the performance of RFBs quickly due to its straightforward and easy implementation (27). Estimation of all parameters of the physics-based electrochemical model for VRSBs has been addressed using two cell systems, which include two different membranes, assuming that both systems have some common characteristics, such as kinetics at the electrodes, the formal potential, and the contact resistance except for diffusivity of ions through the membranes. Firstly, a reference Nafion 115 membrane is used. As diffusion coefficients of vanadium ions for a Nafion 115 membrane are available in

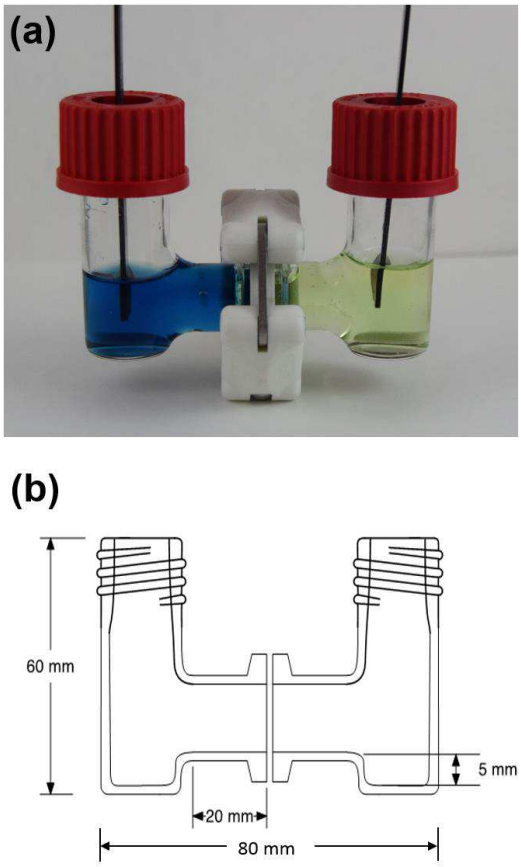

Figure 1. Schematic of the laboratory-scale VRSB system. (a) An actual image of the system for a discharge state. The blue electrolyte represents VO^{2+} (positive) and the green electroltye represents V^{3+} (negative). (b) Specification of the system. The static cell system has advantages of being easy and simple to implement and a quick understanding of the performance of the RFBs. Coupling with electrochemical engineering models for VRSBs helps modelers estimate parameters and analyze cell performance efficiently.

the literature, this information is utilized to estimate other cell system parameters, such as cell resistance and rate constants in the static cell model. The effects of diffusion and migration of ions in the system, which cause capacity fade/loss to the battery, have been analyzed based on the obtained information. Moreover, it has been shown that diffusion coefficients of vanadium ions for other membranes can be estimated based on the estimated parameters in the Nafion 115 system. Using this concept, four vanadium ions' diffusion coefficients of a Nafion XL membrane, which are not available in the literature, have been estimated. Once the parameters have been obtained, one can use the kinetic and transport parameters for simulating redox battery system as well.

Experimental

Materials

Vanadium (IV) oxide sulfate hydrate ($VOSO_4 \cdot xH_2O$) (28) and an aqueous sulfuric acid solution (H_2SO_4) (29) were purchased from Aldrich and used as received. Nafion XL (30) and Nafion 115 (31) membranes were purchased from DuPont and used after pretreatment using

distilled deionized water (DDW) and an aqueous sulfuric acid solution at 80°C for 30 minutes, respectively. POCO graphite electrodes were purchased from Saturn Industries (32).

Instrumentation

The performance of the static cell was obtained at different C-rates, using a Solartron SI 1287 potentiostat (33).

The static cell system

The H-cell (Adams and Chittenden Scientific Glass) (34) consists of a positive and a negative chamber as shown in Figure 1. A membrane is located between these two chambers and the membrane is in contact with the electrolytes of the half-cell. The volume of the electrolytes at the positive and the negative chamber is 10 ml each. Two graphite electrodes with specific reaction surface (1cm × 1cm × 0.1cm) are vertically placed in the center of each chamber and fixed with the plastic caps of the H-cell. There are rubber gaskets inside these plastic caps and silicon is attached to the gaps between the electrode and the gasket to prevent oxygen leakages from outside the system.

Preparation of electrolytes

Sulfuric acid solution (H_2SO_4, 6.73 mL) was slowly added to 7.5mL of DDW, and the final volume was adjusted to 30 mL using DDW to prepare 4M sulfuric acid solution (H_2SO_4). 0.603g of vanadium (IV) oxide sulfate hydrate ($VOSO_4 \cdot xH_2O$) was added very slowly and stirred at 60°C for 1 hour. The hydration of the vanadium oxide sulfate ($VOSO_4$) was determined by Karl Fischer titration using a Mettler Toledo C20 Coulometric KF Titrator with a DO308 oven attachment (35). The instrument was located inside of a dry room where the dew point is -64ºF. Karl Fisher showed two water molecules were hydrated to one vanadium oxide sulfate ($VOSO_4 \cdot 2H_2O$), and the molecular weight (201.042 g/mol) was calculated based on the indication. 30 mL of 0.1M vanadium (IV) oxide sulfate ($VOSO_4$) in an aqueous 4M sulfuric acid solution (H_2SO_4) was prepared. Next, 10 mL of 0.1M vanadium (IV) oxide sulfate ($VOSO_4$) in an aqueous 4M sulfuric acid solution (H_2SO_4) was added to the positive and negative chamber, respectively. The static cell system with Nafion 115 membrane was slowly charged at C/20 ratio to convert VO^{2+} to V^{3+} at the anode and VO^{2+} to VO_2^+ at the cathode. When the upper limit voltage of 1.7V was exceeded, the charge was set to be terminated, and 93.9% V^{3+}/6.1% VO^{2+} electrolytes at the negative chamber were achieved by the coulombic calculation. After that, VO^{2+}/VO_2^+ electrolytes at the positive chamber were drained and refilled with a new 10 mL of 0.1 M VO^{2+} in 4 M sulfuric acid solution (H_2SO_4).

Cell operation

For the Nafion 115 system**,** a typical CC-CV profile (CC: Constant Current, CV: Constant Voltage) was applied (maximum voltage: 1.7V). Once the static cell voltage was reached at 1.7V, it was charged with the CV until the applied current is saturated. That is, CV continued until the exponentially decaying applied current stopped decreasing. For discharging, the CC profile was applied. The CC-CV profile was used to analyze the cell systems' performance at different C-rates (C/20 and C/30), making the cell systems to reach full capacity and study the effects of diffusion and migration. For the Nafion XL cell system, we focused on parameter estimation on diffusion coefficients of the membrane, assuming that all cell system

parameters are the same with the Nafion 115 system except for the ions' diffusion distance, the potential gradient inside a membrane, and diffusion coefficients through the membrane. For charging and discharging, therefore, a CC profile (C/30) was applied to the static cell system. The temperature of the H-cell was maintained at 25°C in the Tenney Environmental Chamber (36). The gas washer, which was filled with water and connected to the argon line and cell system, minimizes evaporation of electrolytes. During the charging and discharging process, a magnetic stirrer was used to make uniform concentrations of the electrolyte in the positive and negative chambers.

Model

Coupling the static cell with zero-dimensional models enhances the easy and straightforward implementation and mitigate computational challenges to simulate models and estimate their parameters. For this reason, a zero-dimensional model was implemented as an example of combining with the proposed estimation approach. Migration effects of vanadium ions through the membrane, the diffusion distance of the membrane, and kinetics at electrodes have been added (3, 9, 13) to a zero-dimensional electrochemical static cell model (demonstrated by *Tang et. al* (11)) which includes diffusion of vanadium ions through the membrane. Parameter estimation techniques were combined with the zero-dimensional model to estimate the parameters appearing in the equations. All relevant equations (Equations 1-4, 9-12, and 17-21 in Table II, III, IV, respectively), variables (Table V), and parameters (Table VI), which are used to model and simulate the VRSB system, are listed in Tables II-VI (3, 9, 11, 13).

Assumption

The following assumptions were made in the static cell model: (i) Side reactions between two different vanadium ions, due to diffusion and migration of ions through the membrane, occur immediately once vanadium ions cross the membrane (3); (ii) Since the gas washer is connected to the static cell system to minimize evaporation of the electrolyte, evaporation of the electrolyte is ignored in the model; (iii) Faraday's law of electrolysis has been utilized to estimate the rate of reactions of vanadium ions at the cathode and anode; (iv) Hydrogen (H_2) and Oxygen (O_2) generations, which evolve at the electrode during charging and discharging, are ignored due to low C-rates (8, 12); (v) Nafion 115 and Nafion XL systems have the identical kinetics at the electrodes, the formal potential, and the contact resistance; (vi) The potential gradient inside a membrane remains constant during battery operation (charging and discharging); (vii) No side reactions take place between other vanadium ions in a membrane.

Diffusion and migration

The undesired but unavoidable crossover of vanadium ions through the membrane, which leads to capacity loss/fade during charging and discharging, is caused by the diffusion, migration, and convection of ions (3). In this static cell model, however, diffusion and migration are considered as the main causes of transport. Convection is one of the important transport phenomena in flow cells, but not relevant in static cells since they contain static electrolytes. The diffusion of vanadium ions occurs at all times regardless of the cell's operating conditions since the driving force of the transport is the concentration gradient between the positive and negative electrolytes (11). In contrast, the net flux of ions through the membrane by migration occurs differently. This is because the driving force of the crossover of ions is to maintain electrical neutrality of the positive and negative electrolytes. When vanadium ions

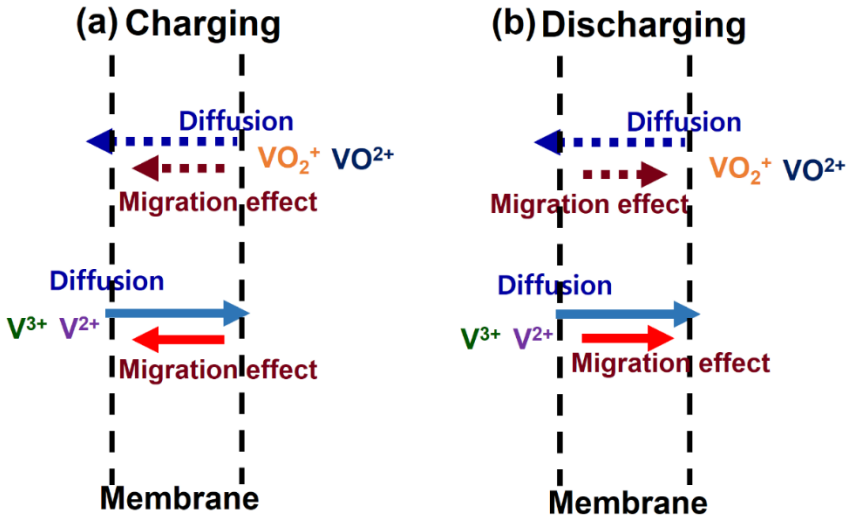

Figure 2. Crossover of vanadium ions through the membrane by diffusion and migration during (a) charging and (b) discharging. A blue colored dotted arrow indicates VO^{2+}/VO_2^+ diffusion (see the first arrow from the top in (a) charge and (b) discharge), a wine colored dotted arrow represents VO^{2+}/VO_2^+ migration (see the second arrow from the top in (a) charging and (b) discharging), a sky-blue colored solid arrow shows V^{2+} / V^{3+} diffusion (see the third arrow from the top in (a) charging and (b) discharging), and a red colored solid arrow represents V^{2+}/V^{3+} migration (see the fourth arrow from the top in (a) charging and (b) discharging). The main transport phenomena of the static system are diffusion and migration. The diffusion of vanadium ions through the membrane has the same direction regardless of charging and discharging and the direction of migration through the membrane is affected by charging / discharging conditions.

cross the membrane, the ions face the potential gradient by migration effects, which slows down or increases the total ion flux as shown in Figure 2. The migration effect occurs from the positive side to the negative side during charging, which is the same direction to the diffusion flux of VO^{2+} and VO_2^+ and the opposite direction to the diffusion flux of V^{2+} and V^{3+}. During discharging, the migration effect occurs from the negative side to the positive side for vanadium ions of the system. In the proposed model, both uni- and anti- directional migration effects (to the diffusion flux) inside a membrane have been added to the zero-dimensional model, assuming that the potential gradient of migration effects remains constant during charging and discharging. After that, the potential gradient is estimated directly. Also, the crossover of the vanadium ions through the membrane causes side reactions in the electrolyte as shown in Figure 3 (11). Once vanadium ions cross the membrane, reactions between two different vanadium ions occur, producing VO^{2+} ions at the positive electrolyte and V^{3+} ions at the negative electrolyte, and this, in turn, causes the capacity loss/fade of the battery (11).

Governing equations

Equations 1-4 and 9-12 of the static cell model, as given in Tables II and III, depict the dynamics of the concentration of vanadium ions including diffusion and migration through the membrane during charging and discharging, respectively (11, 13). This is a system of eight Ordinary Differential Equations (ODEs). In Tables II and III, mass balance equations, consisting of the rate of accumulation of ions, the rate of ions entering the opposite chamber, the rate of ions flowing out from their own chamber, and the rate of loss or generation of ions,

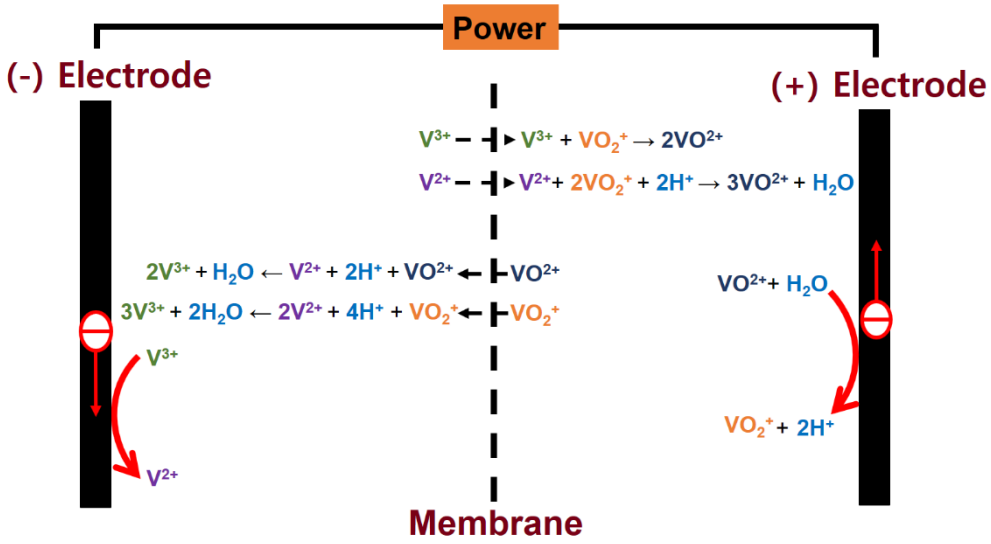

Figure 3. Side reactions caused by crossover of vanadium ions through the membrane durging charging. One mole of V^{2+}, which moves across the membrane from the negative electrolyte, reacts with two moles of VO_2^+ in the positive electrolytes producing three moles of VO^{2+}. One mole of V^{3+} crossover from the negative electrolyte causes a chemical reaction with one mole of VO_2^+ producing two moles of VO^{2+} in the positive electrolyte. Similarly, in the negative electrolyte, two moles of V^{3+} are produced by a chemical reaction between one mole of V^{2+} and one mole of VO^{2+}, which moves from the positive electrolyte, and three moles of V^{3+} are produced by a chemical reaction between two moles of V^{2+} and one mole of VO_2^+, which moves from the positive electrolyte.

were established for vanadium ions. In other words, the rate of accumulation of each vanadium ion species (V^{2+}, V^{3+}, VO^{2+}, and VO_2^+) is the sum of the rate of production of the vanadium ions by side reactions, the rate of outflow into the opposite chamber, and the rate of generation or loss at the electrode by the electrochemical reactions.

Additional equations

Table IV presents additional equations including the cell voltage, the open circuit voltage, and the overpotential used in the model (9, 11, 13). The cell voltage given by Equation 17 is used in the static cell model (11). The formal potential is used to calculate open circuit voltage of the static cell system as given in Equation 18. To use the formal potential, the proton concentration is removed from the logarithmic term in the Nernst Equations (11). The concentration of hydrogen ions in the positive half-cell electrolyte is not known accurately since several ionic equilibria affect the equilibrium concentrations of all the ionic species in the VRSB electrolyte (11). The overpotential at the positive and negative electrodes, including the activation barrier, is calculated as given in Equations 19 and 20, and a charge transfer coefficient of 0.5 is applied to the overpotential (9). Equation 21 represents the conductivity of the membrane (37).

Parameter Estimation

The model parameters are fitted with the experimental data to estimate their values using

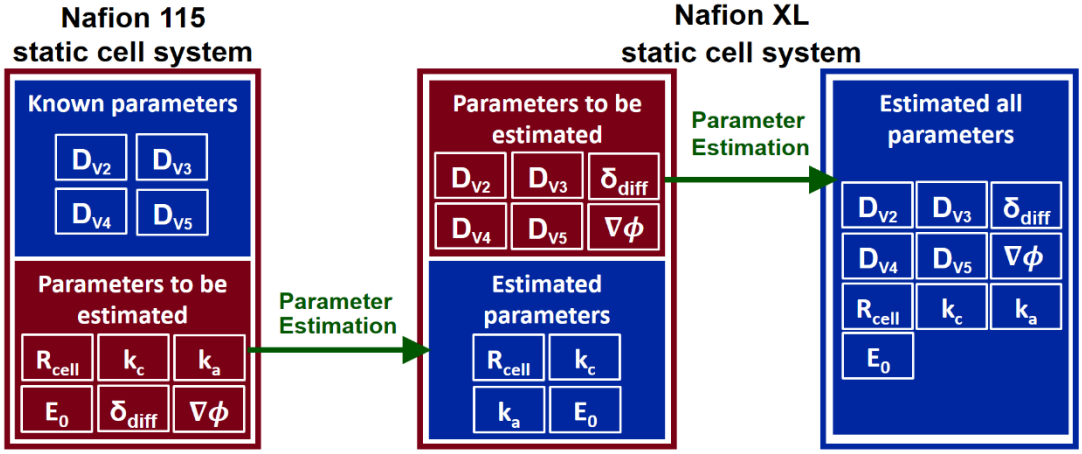

Figure 4. Parameter estimation of the static cell system with charging/ discharging curves at different C-rates. We show a way of estimating all parameters in a model, which can help analyze and study the performance of the cell system.

mathematical optimization techniques. There are ten parameters in the model, which are estimated by the parameter estimation approach, e.g., diffusion coefficients of four different vanadium ionic species for membranes, the contact resistance of the cell, two reference rate constants at cathode and anode, the formal potential, the diffusion distance of the membrane, and the potential gradient inside the membrane. Given certain realistic values of these parameters, the model can be simulated to predict the values of voltage at certain time intervals. The final estimated parameters are obtained by solving an optimization problem where the sum of squares of the differences in the voltage outputs between the model and experiment divided by the total number of experimental data points (known as the Mean Square Error, MSE) for the first cycle (charging and discharging) of the system is minimized, and unknown parameters are used as decision variables (38). The objective of the optimization approach can be expressed as follows:

$$\min \frac{1}{N}\sum_{j=1}^{N}[V_{exp,j} - V_{model,j}]^2 \qquad [22]$$

where N is the total number of experimental data points for charging and discharging, $V_{exp,j}$ and $V_{model,j}$ indicate the experimental and model predicted voltage value of the static cell for the j^{th} data point, respectively. In this paper, the number of 200 voltage data for charge and discharge was collected at regular time intervals. The optimization routine uses several values of the optimizing parameters iteratively before choosing the optimal values for which the objective function (as given in equation 22) subject to model equations, initial conditions, and bounds for the parameters is minimized. The parameter estimation of ten parameters is performed with two cell systems. In each of the system, some parameters are known a priori while other parameters are estimated through the parameter estimation approach as shown in Figure 4. The initial guesses, bounds, converged parameters, and minimized MSE are summarized in Table VII, and the values in Table VII were rounded off to the fourth decimal place. The trial-and-error method has been utilized to obtain initial guesses and lower/upper bounds in this optimization problem (39). Initial guesses were set up based on prior information

(e.g., lower bound of diffusion distance is membrane thickness), and lower and upper bounds were adjusted based on the initial guesses (up to 20% from initial guesses) to the identify minimized MSE. Analyses and studies of simulations and optimizations in this work were carried out on a workstation with dual 8-core, 3.10GHz Intel Xeon processors, 32.0 GB RAM using the NLPsolve (optimization method: nonlinearsimplex, and evaluation limit: maximum) (40) and Globalsolve (evaluation limit: maximum) in optimization package of the Maple® software (41).

The Nafion 115 cell system

The system equipped with a Nafion 115 membrane has been used since the values for the diffusion coefficients of the four vanadium ionic species through this membrane are known from the literature (22). Using this information, the remaining six parameters (contact resistance of the cell system, two reference rate constants at electrodes, the formal potential, the diffusion distance, and the potential gradient) can be estimated through the parameter estimation approach. Parameter estimation has been simultaneously carried out using four experimental voltage profiles of charging and discharging protocols for the first cycle (CC-CV charging and CC discharging for two different C-rates at C/20 and C/30). Also, for the best performance of the optimization problem, the diffusion distance and reference rate constants are expressed in term of an exponential function ($k_c = e^{-A}$, $k_a = e^{-B}$, and $\delta_{diff} = e^{-C}$), and indices (A, B, and C) of the exponential function are used as optimizing variables since the original parameters (k_c, k_a, and δ_{diff}) are too small scale (~10^{-6}) to identify proper optimization values. In this section, however, the original parameters (k_c, k_a, and δ_{diff}) are presented for initial guesses, lower and upper bounds, and converged values. The indices values can be identified by taking the logarithm function.

Initial guesses. The initial guesses for the diffusion distance, the potential gradients at C/30 and C/20, reference rate constants at positive and negative electrodes, the contact resistance, and the formal potential were 136.389 um, 0.73×10^{-4} V/um, 0.105×10^{-3} V/um, 5.404×10^{-7} m/s, 2.212×10^{-6} m/s, 13.810 Ω, 1.436 V.

Lower and upper bounds. The lower and upper bounds for the diffusion distance were 127 to 150.733 um. The bounds for the potential gradients at C/30 and C/20 were given as 0.7×10^{-4} to 0.75×10^{-4} V/um and 0.1×10^{-3} and 0.11×10^{-3} V/um, respectively. The upper and lower bounds for reference rate constants at positive and negative electrodes were 5.044×10^{-7} to 6.160×10^{-7} m/s and 1.851×10^{-6} to 2.260×10^{-6} m/s, respectively. The upper and lower bounds for the contact resistance were 12 to 15 Ω. The bound for the formal potential was given as 1.43 to 1.45 V.

Converged parameters**.** The converged parameters for the diffusion distance, the potential gradients at C/30 and C/20, reference rate constants at positive and negative electrodes, the contact resistance, and the formal potential are 147.824 um, 0.749×10^{-4} V/um , 0.1×10^{-3} V/um , 0.580×10^{-6} m/s, 2.255×10^{-6} m/s, 14.454 Ω, and 1.445 V, respectively. Also, the minimized MSE was 10.627 mV.

The Nafion XL cell system

Voltage outputs from the model are fitted to experimental voltage data at C/30 during the

first cycle. By doing this, diffusion coefficients of vanadium ions for other membranes, which have not yet been investigated, are estimated based on the predetermined other parameters in the Nafion 115 cell system. For example, the Nafion XL membrane equipped static cell system has been considered, where diffusion coefficients have not been identified. While cell system parameters, including the contact resistance of the cell system, two reference rate constants at electrodes, and the formal potential remain the same as obtained in the Nafion 115 system, other six parameters including four diffusion coefficients of the ionic species through the Nafion XL membrane, the diffusion distance of the Nafion XL membrane, and the potential gradient inside the membrane are estimated through the proposed parameter estimation approach. The diffusion distance and diffusion coefficients of four ionic species are expressed in terms of exponential functions as well, where the indices appearing to the power of the number e are used as the parameters for optimization. In this section, the original parameters (the diffusion distance and diffusion coefficients of four ionic species) are reported for initial guesses, lower and upper bounds, and converged values, but indices of exponential function can be identified by taking the logarithm function.

Initial guesses. The initial guesses for the diffusion distance, the potential gradient, and four diffusion coefficients of V^{2+}, V^{3+}, VO^{2+}, and VO_2^{+} were 100um, 0.58×10^{-4} V/um, 9.120×10^{-12} m^2/s, 3.981×10^{-12} m^2/s, 2.428×10^{-11} m^2/s, and 1.738×10^{-11} m^2/s, respectively.

Lower and upper bounds. The lower and upper bounds for the diffusion distance were 82.724 to 102.055 um. The bound for the potential gradient was given as 0.55×10^{-4} to 0.60×10^{-4} V/um. The upper and lower bounds for diffusion coefficients of V^{2+}, V^{3+}, VO^{2+}, and VO_2^{+} were 7.933×10^{-12} to 9.309×10^{-12} m^2/s and 3.099×10^{-12} to 4.183×10^{-12} m^2/s, 1.991×10^{-11} to 3.185×10^{-11} m^2/s, and 1.696×10^{-11} to 1.783×10^{-11} m^2/s, respectively.

Converged parameters. The converged parameters for the diffusion distance, the potential gradient, and four diffusion coefficients of V^{2+}, V^{3+}, VO^{2+}, and VO_2^{+} are 101.961 um, 0.560×10^{-4} V/um, 8.699×10^{-12} m^2/s, 3.632×10^{-12} m^2/s, 2.597×10^{-11} m^2/s, and 1.740×10^{-11} m^2/s, respectively. Also, the minimized error was 0.693 mV.

Results and Discussion

The objective of this paper is to show that redox battery performance can be studied and analyzed using the optimization-based robust modeling framework, including physics-based electrochemical models and parameter estimation techniques. Accordingly, the comparison of voltage profiles between model predictions and experimental data and the predicted vanadium ions concentration are presented in Figure 5, 6, and 7. This section also discusses how the proposed approach can contribute to the RFB model development, providing estimation results of a recently published zero-dimensional model which includes only uni-directional migration effects (13). The importance and limitations of the proposed work and further works will be discussed as well.

The Nafion 115 cell system

The coulombic efficiency of the Nafion 115 system is 0.73 at C/30 and 0.81 at C/20 as shown in Figure 5. It shows that the higher current rates give the higher coulombic efficiency (42). Figures 5a and 5b also illustrate the effects of migration and diffusion of the static cell system. To study and analyze the effects of those two main transport phenomena through the

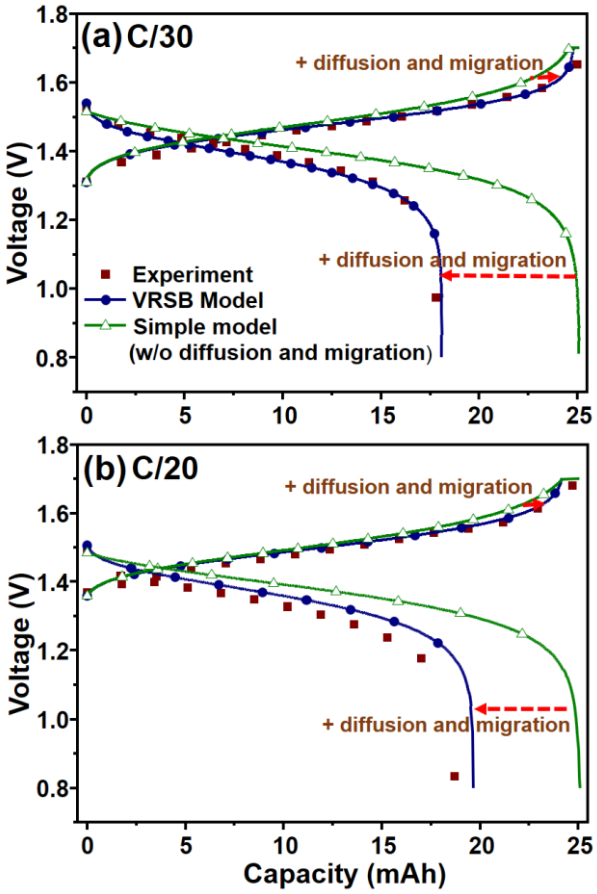

Figure 5. Comparison of voltage profiles between battery model outputs and experimental data from the static cell system including Nafion 115, and analysis of effects of diffusion and migration, using the simple model. Voltage profiles at (a) C/30 and (b) C/20 (Experimental data: wine color and filled square dots, the VRSB model: blue color and filled circle plot, and the simple model: green color and empty triangle plot). Parameters were simultaneously estimated at C/20 and C/30, minimizing the mean of the sum-of-squared differences between the model and experiment outputs.

membrane, the simple model, which does not include diffusion and migration, is presented. There is no crossover of ions through the membrane in the simple model. In the simple model, therefore, Equations 5-8 and 13-16 in Table II and III are used for charging and discharging, respectively, with Equations 17-21 in Table IV and the parameters in Table VI and VII. In Figure 5, the charging profile of the VRSB model, including diffusion and migration, is longer than that of the simple model, and the reverse is found for the discharging profile. Partial self-discharge of vanadium ions through the membrane is one of the main reasons for this capacity loss. To study this capacity loss in detail, Figure 6 describes the comparison of the predicted concentration of vanadium ions between the VRSB and simple model. Ideally, for example, V^{2+} ions should only be generated from V^{3+} ions through an electrochemical reaction at the negative electrode during charging (*see Figure 6b*). In real VRSB systems, however, V^{2+} ions are continuously depleted in negative electrolytes due to side reactions with VO^{2+}/VO_2^+ ions and crossover of V^{2+} ions through the membrane (*see Figure 6a*). Likewise, VO_2^+ ions should be only produced for charging (*see Figure 6d*), but they are also depleted in the positive electrolytes because of their crossover and side reactions giving rise to VO^{2+} ions (*see Figure*

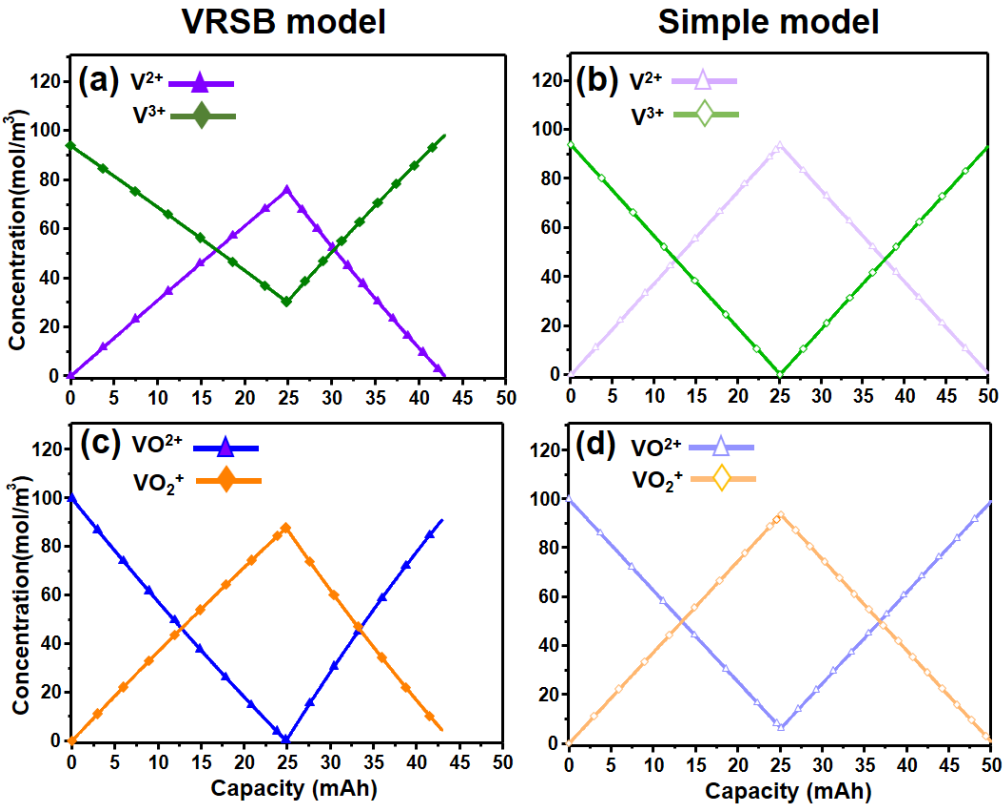

Figure 6. Comparison of predicted concentration of the different vanadium ions between the VRSB model and simple model at C/30. (a) V^{2+} (purple color and filled triangle) and V^{3+} (green color and filled diamon) concentration profiles from the VRSB model at C/30, (b) V^{2+} (light purple color and empty triangle) and V^{3+} (light green color and empty diamon) concentration profiles from the simple model at C/30, (c) VO^{2+} (blue color and filled triangle) and VO_2^+ (orange color and filled diamond) concentration profiles from the VRSB model at C/30, and (d) VO^{2+} (light blue color and empty triangle) and VO_2^+ (light orange color and empty diamond) concentration profiles from the simple model at C/30. An imbalance of the vanadium ion concentration between the positive and negative electrolytes causes capacity loss/fade of VRSB/VRFBs.

6c). The self-discharge of vanadium ions, which happens during charging, causes a slower charge until the cell is achieved at the maximum voltage. In contrast, this self-discharge leads to faster discharge and shorter discharge time. During discharge, V^{2+} and VO_2^+ ions are depleted due to electrochemical reactions at the negative electrode and their side reactions with other vanadium ions and crossover through the membrane, thereby dropping the concentration of V^{2+} and VO_2^+ ions faster (*see Figure 6a and 6c*). For this reason, the self-discharge of vanadium ions, which happens during discharging, causes a faster discharge until the cell is achieved at the minimum voltage. Importantly, the VRSBs/VRFBs do not produce any inert third compound, such as Li- ion SEI/plating, that can cause irreversible capacity loss (43). Rather, side reactions in VRSBs/VRFBs are disproportionate reactions, which convert vanadium ions from one oxidation state to another state (11).

The Nafion XL cell system

Figure 7a presents the comparison of voltage profiles between model outputs and

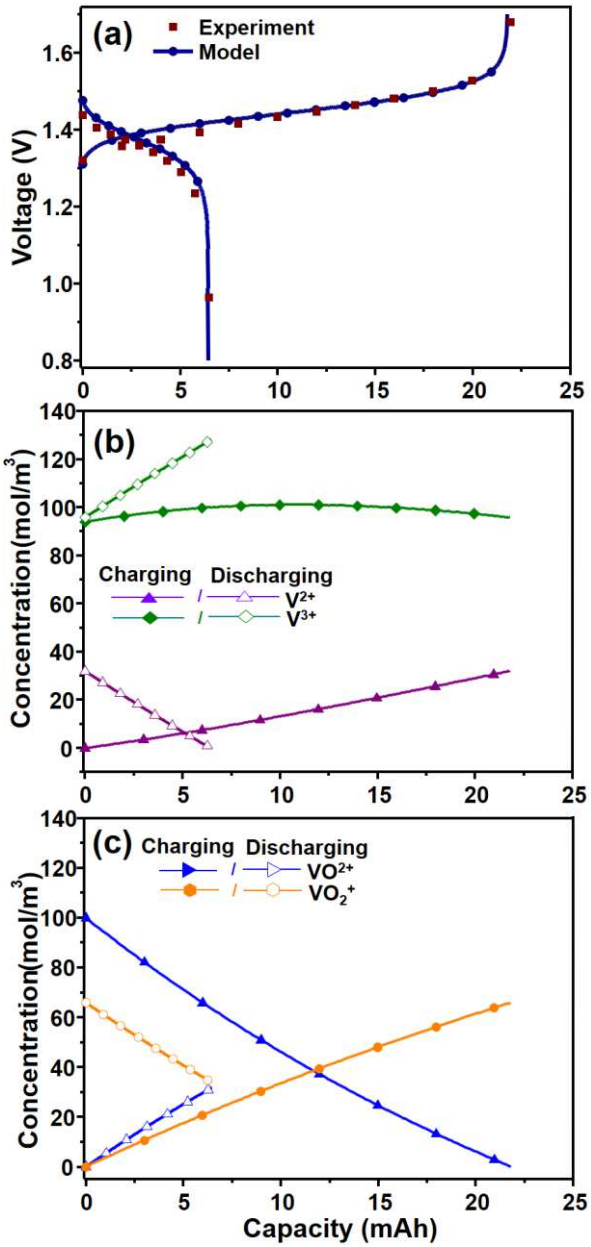

Figure 7. Comparison of voltage profiles between battery model outputs and experimental data, and predicted vanadium ion concentrations vs. capacity, for the static cell system including Nafion XL membrane at the first cycle. (a) Voltage profiles from experiment data (wine color and filled square) and model outputs (blue color and filled circle) at C/30 (b) V^{2+} (charge: green color and filled diamond, and discharge: green color and empty diamond) and V^{3+} (charge: purple color and filled triangle, and discharge: purple color and empty triangle) concentration profiles at C/30. (c) VO^{2+} (charge: blue color and filled triangle, and discharge: blue color and empty triangle) and VO_2^+ (charge: orange color and filled diamond, and discharge: orange color and empty diamond) concentration profiles at C/30. Parameters were estimated at C/30 based on cell system parameters predetermined in the Nafion 115 system, minimizing the mean of sum-of-squared differences between the model and experiment outputs.

experimental data. Figures 7b and 7c show the predicted concentration of V^{2+}, V^{3+}, VO^{2+}, and VO_2^+ ions of the static cell system having Nafion XL membrane. Like the Nafion 115 system,

the change in concentration of V^{2+}/V^{3+} ions is smaller than that of VO^{2+}/VO_2^{+} ions during charging, and the reverse is found during discharging**.** The imbalance of vanadium ion concentration between the positive and negative electrolytes causes capacity loss/fade of VRSBs. The imbalance of the Nafion XL system is more severe than the system of Nafion 115.

Importance of proposed work

The proposed parameter estimation technique can be used as a way to track the effects of capacity loss/fade. As we mentioned earlier, one of the main reasons of the redox batteries' capacity loss/fade is ions' crossover through the membrane (11), and this can be linked to transport and kinetic parameters. The proposed optimization-based approach can be used to update the transport and kinetic parameters or any degradation inputs of redox batteries within a short period. Any mismatch between model and data over cycles can be resolved with the updated parameters, and controls of the redox batteries with precise predictions based on the proposed work might lead to longer battery life and lower battery cost.

Conclusion

This work is an attempt to estimate all parameters of physics-based electrochemical engineering models for VRSBs. This study used a zero-dimensional electrochemical engineering model, which includes mass balance equations of vanadium ions in addition to the other equations covering the aspects of cell voltage, formal and overpotential, the diffusion distance, the potential gradient inside a membrane, etc. This work reports that VRSB/VRFB system can be studied and analyzed in detail based on the parameter estimation approaches, using physics-based electrochemical models. This work provides a way to study and analyze other RFBs based on parameter estimation techniques. The proposed approach of parameter estimation is very generic and can be extended for estimation of parameters for other RFB models incorporating different chemistry as well as complexity (0-D to 3-D).

Acknowledgements

This work was supported by the Clean Energy Institute located in University of Washington, Seattle and Washington Research Foundation. The battery modeling work has been supported by the Assistant Secretary for Energy Efficiency and Renewable Energy, Office of Vehicle Technologies of the U. S. Department of Energy through the Advanced Battery Material Research (BMR) Program (Battery500 Consortium). The battery experimental work has been supported by program manager Dr. Imre Gyuk through the U.S. Department of Energy, Office of Electricity Delivery and Energy Reliability. Sandia National Laboratories is a multi-mission laboratory managed and operated by National Technology and Engineering Solutions of Sandia, LLC., a wholly owned subsidiary of Honeywell International, Inc., for the U.S. Department of Energy's National Nuclear Security Administration under contract DE-NA0003525.

References

1. K. T. Cho, P. Ridgway, A. Z. Weber, S. Haussener, V. Battaglia and V. Srinivasan, *Journal of The Electrochemical Society*, **159**, A1806 (2012).
2. *VanadiumCorp. "Integrity, Originality, Service."Redox Flow Batteries Charge Forward. Ios Services, Sept.-Oct. 2016. Web. 15 July 2017. Available:* http://www.iosgeo.com/en/news/news-from-our-clients/redox-flow-batteries-charge-forward/.
3. K. Knehr, E. Agar, C. Dennison, A. Kalidindi and E. Kumbur, *Journal of The Electrochemical Society*,

159, A1446 (2012).
4. D. You, H. Zhang and J. Chen, *Electrochimica Acta*, **54**, 6827 (2009).
5. K. Knehr and E. Kumbur, *Electrochemistry Communications*, **13**, 342 (2011).
6. H. Al-Fetlawi, A. Shah and F. Walsh, *Electrochimica Acta*, **55**, 78 (2009).
7. G. Merei, S. Adler, D. Magnor, M. Leuthold and D. U. Sauer, *Energy Procedia*, **46**, 194 (2014).
8. H. Al-Fetlawi, A. Shah and F. Walsh, *Electrochimica Acta*, **55**, 3192 (2010).
9. A. Shah, R. Tangirala, R. Singh, R. Wills and F. Walsh, *Journal of the Electrochemical society*, **158**, A671 (2011).
10. A. Shah, M. Watt-Smith and F. Walsh, *Electrochimica Acta*, **53**, 8087 (2008).
11. A. Tang, J. Bao and M. Skyllas-Kazacos, *Journal of Power Sources*, **196**, 10737 (2011).
12. A. Shah, H. Al-Fetlawi and F. Walsh, *Electrochimica Acta*, **55**, 1125 (2010).
13. P. A. Boettcher, E. Agar, C. Dennison and E. C. Kumbur, *Journal of The Electrochemical Society*, **163**, A5244 (2016).
14. Y. Lei, B. Zhang, B. Bai and T. S. Zhao, *Journal of Power Sources*, **299**, 202 (2015).
15. Y. A. Gandomi, T. A. Zawodzinski and M. M. Mench, *ECS Transactions*, **61**, 23 (2014).
16. D. A. Beck, J. M. Carothers, V. R. Subramanian and J. Pfaendtner, *AIChE J*, **62**, 1402 (2016).
17. S. B. Lee, C. Pathak, V. Ramadesigan, W. Gao and V. R. Subramanian, *Journal of The Electrochemical Society*, **164**, E3026 (2017).
18. Z. Wei, T. M. Lim, M. Skyllas-Kazacos, N. Wai and K. J. Tseng, *Applied Energy*, **172**, 169 (2016).
19. R. L. Fares, J. P. Meyers and M. E. Webber, *Applied Energy*, **113**, 189 (2014).
20. Z. Wei, K. J. Tseng, N. Wai, T. M. Lim and M. Skyllas-Kazacos, *Journal of Power Sources*, **332**, 389 (2016).
21. E. Wiedemann, A. Heintz and R. Lichtenthaler, *Journal of membrane science*, **141**, 215 (1998).
22. C. Sun, J. Chen, H. Zhang, X. Han and Q. Luo, *Journal of Power Sources*, **195**, 890 (2010).
23. J. Li, L. Wang, C. Lyu, H. Wang and X. Liu, *Journal of Power Sources*, **307**, 220 (2016).
24. M. Skyllas-Kazacos and L. Goh, *Journal of membrane science*, **399**, 43 (2012).
25. D. Aaron, C.-N. Sun, M. Bright, A. B. Papandrew, M. M. Mench and T. A. Zawodzinski, *ECS Electrochemistry Letters*, **2**, A29 (2013).
26. M. Miller, A. Bourke, N. Quill, J. Wainright, R. Lynch, D. Buckley and R. Savinell, *Journal of The Electrochemical Society*, **163**, A2095 (2016).
27. H. D. Pratt, N. S. Hudak, X. Fang and T. M. Anderson, *Journal of Power Sources*, **236**, 259 (2013).
28. *Sigma-Aldrich. Web. 15 July 2017.* *Available:* http://www.sigmaaldrich.com/catalog/product/aldrich/233706?lang=en®ion=US.
29. *Sigma-Aldrich. Web. 16 July 2017.* *Available:* http://www.sigmaaldrich.com/catalog/product/aldrich/339741?lang=en®ion=US.
30. S. Shi, A. Z. Weber and A. Kusoglu, *Journal of Membrane Science*, **516**, 123 (2016).
31. S. Motupally, A. J. Becker and J. W. Weidner, *Journal of The Electrochemical Society*, **147**, 3171 (2000).
32. *Graphite. Web. 15 July 2017. Available:* http://poco.com/MaterialsandServices/Graphite.aspx.
33. *AMETEK SI. Web. 15 July 2017. Available:* http://www.ameteksi.com/products/potentiostats/single-channel/12xx-series.
34. *Adams & Chittenden Scientific Glass Home. Web. 16 July 2017.* *Available:* http://www.adamschittenden.com/index.php.
35. *METTLER TOLEDO. Web. 11 March, 2018. Available:* www.mt.com/us/en/home/perm-lp/market-organizations/usa/maw_ANA_karl_fischer_titrators_1.html.
36. *Tenney Environmental Walk In Room."Manufacturer of Industrial Ovens and Test Chambers. Web. 16 July 2017. Available: https://*www.thermalproductsolutions.com/product/tenney-environmental-walk-in-room.
37. T. E. Springer, T. Zawodzinski and S. Gottesfeld, *Journal of the Electrochemical Society*, **138**, 2334 (1991).
38. V. Ramadesigan, K. Chen, N. A. Burns, V. Boovaragavan, R. D. Braatz and V. R. Subramanian, *Journal of The Electrochemical Society*, **158**, A1048 (2011).
39. J. V. Beck and K. J. Arnold, *Parameter estimation in engineering and science*, James Beck (1977).
40. *Maplesoft. Web. 24 January 2018.* *Available:https://*www.maplesoft.com/support/help/maple/view.aspx?path=Optimization%2fGeneral%2fOptions.
41. J. D. Pintér, D. Linder and P. Chin, *Optimisation Methods and Software*, **21**, 565 (2006).
42. A. Z. Weber, M. M. Mench, J. P. Meyers, P. N. Ross, J. T. Gostick and Q. Liu, *Journal of Applied Electrochemistry*, **41**, 1137 (2011).
43. P. Verma, P. Maire and P. Novák, *Electrochimica Acta*, **55**, 6332 (2010).
44. A. Tang, J. Bao and M. Skyllas-Kazacos, *Journal of Power Sources*, **216**, 489 (2012).

TABLE I. Selected Physics-based Electrochemical Engineering Models of Vanadium Redox Flow Batteries

Model	Ions and molecules included in models									Ions and molecules transport						Gassing side reactions		Thermal effects	Transport theory	Key points	Year (Ref.)
										across electrodes			through the membrane								
	V^{2+}	V^{3+}	VO^{2+}	VO_2^+	H^+	OH^-	HSO_4^-	SO_4^{2-}	H_2O	Diff.	Mig.	Conv.	Diff.	Mig.	Conv.	H_2	O_2				
Zero-dimensional models																					
Shah *et. al.*	O	O	O	O	O	X	X	X	O	N/A - Zero-dimensional models assume that bulk electrolyte transport happens across the membrane from positive and negative electrodes. - There is concentration gradient across electrodes in real system, but zero-dimensional models are important for control and prediction for long cycles			X H^+: No constraints H_2O: Osmotic drag	X	X	X	X	Isothermal	Not Applicable	Allowed only H^+ and H_2O crossover through the membrane	2011 (9)
Tang *et. al.*	O	O	O	O	X	X	X	X	X				O V^{2+}, V^{3+}, VO^{2+}, and VO_2^+	X	X	Used current efficiency factor		Isothermal	Dilute solution	Demonstrated the static cell model	2011 (11)
Tang *et. al*	O	O	O	O	X	X	X	X	X				O V^{2+}, V^{3+}, VO^{2+}, and VO_2^+	X	X	X	X	Thermal	Dilute solution	Coupled thermal effects with mass balance equations	2012 (44)
Boettcher *et. al.*	O	O	O	O	O	X	O	O	O				O All ions except for OH^-, and SO_4^{2-}	O	O	X	X	Isothermal	Dilute solution	Limitation is uni-directional flux for migration.	2016 (13)
One-dimensional models (assuming bulk electrolytes at positive and negative)																					
Gandomi *et. al.*	X	X	X	X	O	X	O	X	O	N/A - One-dimensional membrane models assume positive and negative have bulk electrolyte transport.			N/A (concentrated solution) H^+, HSO_4^-, and H_2O			X	X	Isothermal	Concentrated solution	Assumed that only H^+, HSO_4^-, and H_2O can cross the membrane	2014 (14)
Lei *et. al.*	O	O	O	O	O	X	O	X	X				O All ions except for SO_4^{2-}, OH^- and H_2O	O	O	X	X	Isothermal	Dilute solution	Included Donnan effects	2015 (15)
Two-dimensional models																					
Shah *et. al.*	O	O	O	O	O	X	O	O	O	O V^{2+}, V^{3+}, VO^{2+}, and VO_2^+	O	O	O H^+, HSO_4^-, and H_2O	O	O	O	X	Isothermal	Dilute solution	No vanadium ions crossover through the membrane and side reactions of the same	2010 (12)
Al-Fetlawi *et. al.*	O	O	O	O	O	X	O	O	O	O V^{2+}, V^{3+}, VO^{2+}, and VO_2^+	O	O	X H^+, HSO_4^-, and H_2O	X	X	X	O	Thermal	Dilute solution		2009 (8)
Knehr *et. al.*	O	O	O	O	O	X	O	O	O	O All ions except for SO_4^{2-}, and OH^-	O	O	O	O	O	X	X	Isothermal	Dilute solution	Implemented improved OCV and Donnan potential	2012 (3)

*Diffusion (Diff.). Migration (Mig.). Convection (Conv.). Not Applicable (N/A).

TABLE II. Governing Equations of All-Vanadium Redox Static Batteries (Charging Process)

Accumulation	=	+ In – Out + Generation/ Loss (Diffusion terms)	(Migration terms)	No.
VRSB Model (Diffusion + Migration)				
$V_r \frac{dC_{V^{2+}}(t)}{dt}$	$= +\frac{j_{app}}{F} A_{elec}$	$-\left(D_{V^{2+}} C_{V^{2+}}(t) + 2D_{VO_2^+} C_{VO_2^+}(t) + D_{VO^{2+}} C_{VO^{2+}}(t)\right)\frac{A_{mem}}{\delta_{diff}}$	$-2\left(D_{VO^{2+}} C_{VO^{2+}}(t) + D_{VO_2^+} C_{VO_2^+}(t) - D_{V^{2+}} C_{V^{2+}}(t)\right)\frac{F}{RT} A_{mem} \nabla\phi$	[1]
$V_r \frac{dC_{V^{3+}}(t)}{dt}$	$= -\frac{j_{app}}{F} A_{elec}$	$-\left(D_{V^{3+}} C_{V^{3+}}(t) - 3D_{VO_2^+} C_{VO_2^+}(t) - 2D_{VO^{2+}} C_{VO^{2+}}(t)\right)\frac{A_{mem}}{\delta_{diff}}$	$+\left(4D_{VO^{2+}} C_{VO^{2+}}(t) + 3D_{VO_2^+} C_{VO_2^+}(t) + 3D_{V^{3+}} C_{V^{3+}}(t)\right)\frac{F}{RT} A_{mem} \nabla\phi$	[2]
$V_r \frac{dC_{VO^{2+}}(t)}{dt}$	$= -\frac{j_{app}}{F} A_{elec}$	$-\left(D_{VO^{2+}} C_{VO^{2+}}(t) - 3D_{V^{2+}} C_{V^{2+}}(t) - 2D_{V^{3+}} C_{V^{3+}}(t)\right)\frac{A_{mem}}{\delta_{diff}}$	$-2\left(D_{VO^{2+}} C_{VO^{2+}}(t) + 3D_{V^{2+}} C_{V^{2+}}(t) + 3D_{V^{3+}} C_{V^{3+}}(t)\right)\frac{F}{RT} A_{mem} \nabla\phi$	[3]
$V_r \frac{dC_{VO_2^+}(t)}{dt}$	$= +\frac{j_{app}}{F} A_{elec}$	$-\left(D_{VO_2^+} C_{VO_2^+}(t) + 2D_{V^{2+}} C_{V^{2+}}(t) + D_{V^{3+}} C_{V^{3+}}(t)\right)\frac{A_{mem}}{\delta_{diff}}$	$-\left(D_{VO_2^+} C_{VO_2^+}(t) - 4D_{V^{2+}} C_{V^{2+}}(t) - 3D_{V^{3+}} C_{V^{3+}}(t)\right)\frac{F}{RT} A_{mem} \nabla\phi$	[4]
Simple model (w/o diffusion and migration)				
$V_r \frac{dC_{V^{2+}}(t)}{dt}$	$= +\frac{j_{app}}{F} A_{elec}$			[5]
$V_r \frac{dC_{V^{3+}}(t)}{dt}$	$= -\frac{j_{app}}{F} A_{elec}$			[6]
$V_r \frac{dC_{VO^{2+}}(t)}{dt}$	$= -\frac{j_{app}}{F} A_{elec}$			[7]
$V_r \frac{dC_{VO_2^+}(t)}{dt}$	$= +\frac{j_{app}}{F} A_{elec}$			[8]

TABLE III. Governing Equations of All-Vanadium Redox Static Batteries (Discharging Process)

Accumulation	=	**+In – Out + Generation/ Loss** (Diffusion terms)	(Migration terms)	**No.**
VRSB Model (Diffusion + Migration)				
$V_r \frac{dC_{V^{2+}}(t)}{dt}$	$= -\frac{j_{app}}{F} A_{elec}$	$-\left(D_{V^{2+}} C_{V^{2+}}(t) + 2D_{VO_2^+} C_{VO_2^+}(t) + D_{VO^{2+}} C_{VO^{2+}}(t)\right)\frac{A_{mem}}{\delta_{diff}}$	$-2\left(D_{V^{2+}} C_{V^{2+}}(t) - D_{VO^{2+}} C_{VO^{2+}}(t) - D_{VO_2^+} C_{VO_2^+}(t)\right)\frac{F}{RT} A_{mem} \nabla\phi$	[9]
$V_r \frac{dC_{V^{3+}}(t)}{dt}$	$= +\frac{j_{app}}{F} A_{elec}$	$-\left(D_{V^{3+}} C_{V^{3+}}(t) - 3D_{VO_2^+} C_{VO_2^+}(t) - 2D_{VO^{2+}} C_{VO^{2+}}(t)\right)\frac{A_{mem}}{\delta_{diff}}$	$-\left(3D_{V^{3+}} C_{V^{3+}}(t) + 4D_{VO^{2+}} C_{VO^{2+}}(t) + 3D_{VO_2^+} C_{VO_2^+}(t)\right)\frac{F}{RT} A_{mem} \nabla\phi$	[10]
$V_r \frac{dC_{VO^{2+}}(t)}{dt}$	$= +\frac{j_{app}}{F} A_{elec}$	$-\left(D_{VO^{2+}} C_{VO^{2+}}(t) - 3D_{V^{2+}} C_{V^{2+}}(t) - 2D_{V^{3+}} C_{V^{3+}}(t)\right)\frac{A_{mem}}{\delta_{diff}}$	$+2\left(3D_{V^{2+}} C_{V^{2+}}(t) + 3D_{V^{3+}} C_{V^{3+}}(t) + D_{VO^{2+}} C_{VO^{2+}}(t)\right)\frac{F}{RT} A_{mem} \nabla\phi$	[11]
$V_r \frac{dC_{VO_2^+}(t)}{dt}$	$= -\frac{j_{app}}{F} A_{elec}$	$-\left(D_{VO_2^+} C_{VO_2^+}(t) + 2D_{V^{2+}} C_{V^{2+}}(t) + D_{V^{3+}} C_{V^{3+}}(t)\right)\frac{A_{mem}}{\delta_{diff}}$	$-\left(4D_{V^{2+}} C_{V^{2+}}(t) + 3D_{V^{3+}} C_{V^{3+}}(t) - D_{VO_2^+} C_{VO_2^+}(t)\right)\frac{F}{RT} A_{mem} \nabla\phi$	[12]
Simple model (w/o diffusion and migration)				
$V_r \frac{dC_{V^{2+}}(t)}{dt}$	$= -\frac{j_{app}}{F} A_{elec}$			[13]
$V_r \frac{dC_{V^{3+}}(t)}{dt}$	$= +\frac{j_{app}}{F} A_{elec}$			[14]
$V_r \frac{dC_{VO^{2+}}(t)}{dt}$	$= +\frac{j_{app}}{F} A_{elec}$			[15]
$V_r \frac{dC_{VO_2^+}(t)}{dt}$	$= -\frac{j_{app}}{F} A_{elec}$			[16]

TABLE IV. Additional Equations of All-Vanadium Redox Static Batteries

Equations	No.
$E_{cell}(t) = E_{cell}^{rev}(t) - j_{app}A_{electrode}R_{contact} - j_{app}\frac{d}{\sigma_{mem}} + \eta_2(t) - \eta_1(t)$	[17]
$E_{cell}^{rev}(t) = E_0 + \frac{RT}{F}\ln\left(\frac{C_{V^{2+}}(t)C_{VO_2^+}(t)}{C_{V^{3+}}(t)C_{VO^{2+}}(t)}\right)$	[18]
$\eta_1(t) = -\frac{2RT}{F}\arcsin\left(\frac{i_{app}}{2Fk_a\sqrt{C_{V^{3+}}(t)C_{V^{2+}}(t)}}\right),\ \eta_2(t) = \frac{2RT}{F}\arcsin\left(\frac{i_{app}}{2Fk_c\sqrt{C_{VO^{2+}}(t)C_{VO_2^+}(t)}}\right)$	[19]
$k_a = k_{a,ref}\exp\left(-\frac{F}{E_0^a}\frac{1}{R}\left(\frac{1}{T_{ref}} - \frac{1}{T}\right)\right),\ k_c = k_{c,ref}\exp\left(-\frac{F}{E_0^c}\frac{1}{R}\left(\frac{1}{T_{ref}} - \frac{1}{T}\right)\right)$	[20]
$\sigma_{mem} = (0.5139\lambda - 0.326)\exp\left(1268\left(\frac{1}{303} - \frac{1}{T}\right)\right)$	[21]

TABLE V. Variables of All-Vanadium Redox Static Batteries

Symbol	Variable	Units
$C_{V^{2+}}(t)$	Concentration of Vanadium (II)	$mol\,m^{-3}$
$C_{V^{3+}}(t)$	Concentration of Vanadium (III)	$mol\,m^{-3}$
$C_{VO^{2+}}(t)$	Concentration of Vanadium (IV)	$mol\,m^{-3}$
$C_{VO_2^+}(t)$	Concentration of Vanadium (V)	$mol\,m^{-3}$
$E_{cell}(t)$	Cell voltage	V
$E_{cell}^{rev}(t)$	Open circuit voltage	V
$\eta_1(t)$	Overpotential at anode	V
$\eta_2(t)$	Overpotential at cathode	V

TABLE VI. Parameters of All-Vanadium Redox Static Batteries

Symbol	Parameter	Values	Units
d	Thickness of membrane - Nafion 115	127×10^{-6}	m
	- Nafion XL	27.5×10^{-6}	
A_{mem}	Cross sectional area of the membrane	1.766×10^{-4}	m^2
A_{elec}	Surface area of the electrode for reaction	2.3×10^{-4}	m^2
V_r	Volume of electrolyte	10^{-5}	m^3
T	Temperature	298	K
i_{app}	Applied current	$C/20: 1.34\times10^{-3}$ $C/30: 0.89\times10^{-3}$	A
j_{app}	Current density	$C/20: 5.826$ $C/30: 3.870$	$A\,m^{-2}$
F	Faraday constant	96485.3365	$s\,A\,mol^{-1}$
λ	The membrane water content	22	
R	Ideal gas constant	8.314	$J\,K^{-1}\,mol^{-1}$
$D_{V^{2+}}$	V^{2+} diffusion coefficient of Nafion 115	0.877×10^{-11}	$m^2\,s^{-1}$
$D_{V^{3+}}$	V^{3+} diffusion coefficient of Nafion 115	0.322×10^{-11}	$m^2\,s^{-1}$
$D_{VO^{2+}}$	VO^{2+} diffusion coefficient of Nafion 115	0.683×10^{-11}	$m^2\,s^{-1}$
$D_{VO_2^+}$	VO_2^+ diffusion coefficient of Nafion 115	0.590×10^{-11}	$m^2\,s^{-1}$
E_0^a	Reference potential at anode reaction	−0.26	V
E_0^c	Reference potential at cathode reaction	1.004	V

TABLE VII. Estimated Parameters of All-Vanadium Redox Static Batteries

Symbol	Parameter	Lower bound	Upper bound	Initial guess	Final value (Units)
$R_{contact}$	Resistance	12	15	13.810	14.454 (Ω)
$k_{c,ref}$	Reference rate constant at positive electrode	5.044×10^{-7}	6.160×10^{-7}	5.404×10^{-7}	0.580×10^{-6} ($m\,s^{-1}$)
$k_{a,ref}$	Reference rate constant at negative electrode	1.851×10^{-6}	2.260×10^{-6}	2.212×10^{-6}	2.255×10^{-6} ($m\,s^{-1}$)
E_0	Formal potential	1.43	1.45	1.436	1.445 (V)
δ_{diff}	Diffusion distance Nafion 115	127	150.733	136.389	147.824 (um)
	Nafion XL	82.724	102.055	100	101.961 (um)
$\nabla\phi$	Potential gradient Nafion 115 at C/30	0.7×10^{-4}	0.75×10^{-4}	0.73×10^{-4}	0.749×10^{-4} (V/um)
	At C/20	0.1×10^{-3}	0.11×10^{-3}	0.105×10^{-3}	0.1×10^{-3} (V/um)
	Nafion XL system	0.55×10^{-4}	0.6×10^{-4}	0.58×10^{-4}	0.559×10^{-4} (V/um)
$D_{V^{2+}}$	V^{2+} diffusion coefficient for Nafion XL	7.933×10^{-12}	9.309×10^{-12}	9.120×10^{-12}	8.699×10^{-12} ($m^2\,s^{-1}$)
$D_{V^{3+}}$	V^{3+} diffusion coefficient for Nafion XL	3.099×10^{-12}	4.183×10^{-12}	3.981×10^{-12}	3.632×10^{-12} ($m^2\,s^{-1}$)
$D_{VO^{2+}}$	VO^{2+} diffusion coefficient for Nafion XL	1.991×10^{-11}	3.185×10^{-11}	2.428×10^{-11}	2.597×10^{-11} ($m^2\,s^{-1}$)
$D_{VO_2^+}$	VO_2^+ diffusion coefficient for Nafion XL	1.696×10^{-11}	1.783×10^{-11}	1.738×10^{-11}	1.740×10^{-11} ($m^2\,s^{-1}$)